J. Plasma Fusion Res. SERIES, Vol. 9 (2010)

Contributions of small scales to statistics of Hall MHD turbulence

Hideaki MIURA

Department of Simulation Science, National Institute for Fusion Science, Gifu 509-5292, Japan

(Received: 18 November 2009 / Accepted: 5 February 2010)

A direct numerical simulation of decaying, homogeneous and isotropic turbulence of the incompressible Hall magnetohydrodynamic equations is carried out to clarify its statistical natures. Contributions of small scales to the statistics are examined. It is shown that the probability density function (PDF) of the enstrophy density is well characterized by the Gaussian distribution when the short wave number coefficients are removed, even though the vortex field shows intermittent structures. It is also shown that the local vortex structures are aligned to the magnetic field lines especially when the turbulent field is under developing and small scales are going to be excited. The alignment is lost in the relaxation process, suggesting the small scale current density field is less affected by the dissipations than the vorticity field.

Keywords: Hall MHD turbulence, statistics, vortex structures

1. Introduction

Plasma turbulence is commonly observed in various phenomena such as solar coronas, solar winds and fusion experiments. Since macroscopic behaviors of plasma turbulence are well described by the one-fluid magnetohydrodynamics (MHD) equations, it is a suitable model to initiate studies of plasma turbulence. MHD turbulence is often characterized by a power-law of energy spectra and/or intermittent structures, as neural fluid turbulence is. While theories of MHD turbulence by Iroshnikov and Kraichnan predict the $k^{-3/2}$ power law of the energy spectrum, observations of solar winds appear to show rather the classical $k^{-5/3}$ Kolmogorov spectrum. (See Ref. [1] and references there in.) The scaling property of the turbulent energy spectra has been extensively studied by means of direct numerical simulation (DNS), too. Although the numerical works provide us invaluable information on turbulence, due to a limited resolution achievable in numerical simulations, the energy spectrum obtained by a DNS of MHD turbulence should be essentially scaled at the near-dissipation range, where one-fluid MHD ordering may not necessarily be appropriate. Thus in order to study properties of turbulence in such small scales, a more precise model is required.

An alternative and the simplest framework of the plasma turbulence might be the Hall MHD equations, in which the Hall term is added to the induction equation. The Hall term is quadratic to the magnetic field and varies some aspects of (non-Hall) MHD turbulence. For example, we expect emergence of the Whistler-Alfvén waves, in stead of the Alfvén waves in non-Hall MHD turbulence [4]. Nonlinear interactions in the non-Hall MHD turbulence is often understood by the collisions of Alfvén waves which propagate along the magnetic field lines, and also by slower dynamics in the direction perpendicular to the magnetic field lines [5–7]. In the Hall MHD turbulence, the interaction time scales and frequency of interactions are altered because high wave number Whistler-Alfvén waves propagate much faster than the Alfvén waves. Then the power spectra and local structures in the Hall MHD turbulence are modified from those of non-Hall MHD turbulence.

In the previous article [3], we have reported some spectral properties of the Hall MHD turbulence through the direct comparison with the non-Hall MHD turbulence of the same dissipative coefficients and the same initial condition. In this article we report results of further numerical analyses on the Hall MHD turbulence. Our interests in this article are vortex structures and their statistical properties with/without small scale Fourier coefficients, because such analyses on scale separations can provide basic information to model the equations in terms of so called eddy viscosity and/or eddy currents, which we often require for various numerical studies. This paper is organized as follows. In Sec.2, a direct numerical simulation of the Hall MHD equations is carried out. Basic information of the simulation and some aspects of the numerical simulations are shown. In Sec.3, statistical properties of the turbulent field are reported. Summary is presented in Sec.4.

2. Direct numerical simulation

A DNS of the decaying, homogeneous and isotropic turbulence of the incompressible Hall MHD equations is carried out in this section. The incompressible Hall MHD equations are described as

$$\frac{\partial V_i}{\partial t} = -\frac{\partial}{\partial x_j}\left(V_iV_j - B_iB_j\right)$$

author's e-mail: miura.hideaki@nifs.ac.jp

$$-\frac{\partial}{\partial x_i}\left(p+\frac{1}{2}B_iB_i\right)+\nu\frac{\partial^2 V_i}{\partial x_j \partial x_j}, \quad (1)$$

$$\frac{\partial V_j}{\partial x_j} = 0, \quad (2)$$

$$\frac{\partial B_i}{\partial t} = \epsilon_{ijk}\frac{\partial}{\partial x_j}[\epsilon_{kmn}\left(V_m-\epsilon j_m\right)B_n-\eta j_k], \quad (3)$$

$$j_i = \epsilon_{ijk}\frac{\partial B_k}{\partial x_j}, \quad (4)$$

where V_i, B_i, j_i are the i-th component of the velocity field vector $\boldsymbol{V}$, the magnetic field vector $\boldsymbol{B}$, and the current density vector $\boldsymbol{j}$, respectively. We also introduce the vorticity vector field $\boldsymbol{\omega}$, of which i-th component is given as $\omega_i=\epsilon_{ijk}\partial V_k/\partial x_j$. The symbols ϵ_{ijk}, ν, η are the Eddington's anti-symmetric tensor, the viscosity and the resistivity.

The equations (1)-(4) are solved numerically by the pseudo-spectral method and the Runge-Kutta-Gill scheme under the triple periodic boundary condition over $(2\pi)^3$ box. The number of grid points is $N^3=512^3$. The aliasing errors in the pseudo-spectral computations are removed by the 2/3-truncation. Because of the 2/3-truncation, the maximum wave number in this simulation is limited to $k_{max}=170$. The Hall parameter, the viscosity and the resistivity are set as $\epsilon=0.05$, $\nu=\eta=2\times10^{-3}$, respectively. The initial conditions are given by the energy spectrum $E_\alpha(k)\propto k^4\exp\left(-2k^2/k_0^2\right)$ ($k_0=2$ is given here) and the random phases for both the velocity vector field and the magnetic vector field.

In this section we see some averaged quantities and energy spectra. (A few of them have been shown in the previous work [3]. We see again for the sake of understanding the nature of turbulence better.) In Fig.1(a), time evolutions of the kinetic energy $E_K=\langle V_iV_i\rangle/2$ (solid line) and the magnetic energy $E_M=\langle B_iB_i\rangle/2$ (dashed line) are shown. The symbol $\langle\cdot\rangle$ denotes the volume average. In Fig.1(a), the total energy $E_T=E_K+E_M$ (dotted line) decays monotonically, while each of E_K and E_M does not behave monotonically because E_K and E_M exchange their energies each other. In Fig.1(b), time evolutions of the enstrophy $Q=\langle\omega_i\omega_i\rangle/2$ and the total current $J=\langle j_ij_i\rangle/2$ are shown. Both Q and J are peaked at $t=T_0\simeq0.5$. Hereafter we make use of the time stamp T_0, and study the turbulent field at $t=T_0/2$, T_0, $2T_0$, $3T_0$ and $4T_0$ in this article. In Fig.1(c), the Taylor's micro-scale Reynolds number R_λ^V for the velocity field and its counter part to the magnetic field $R_{\lambda'}^M$ are shown. At $t=T_0$, $R_\lambda^V\simeq89$ and $R_{\lambda'}^M\simeq93$. A difference between the two Reynolds numbers is clear after $t=T_0$. The magnetic Reynolds number $R_{\lambda'}^M$ is almost constant for $t\geq T_0$, while R_λ^V keeps decaying slowly.

In Figs.2(a) and (b), the kinetic energy spectrum

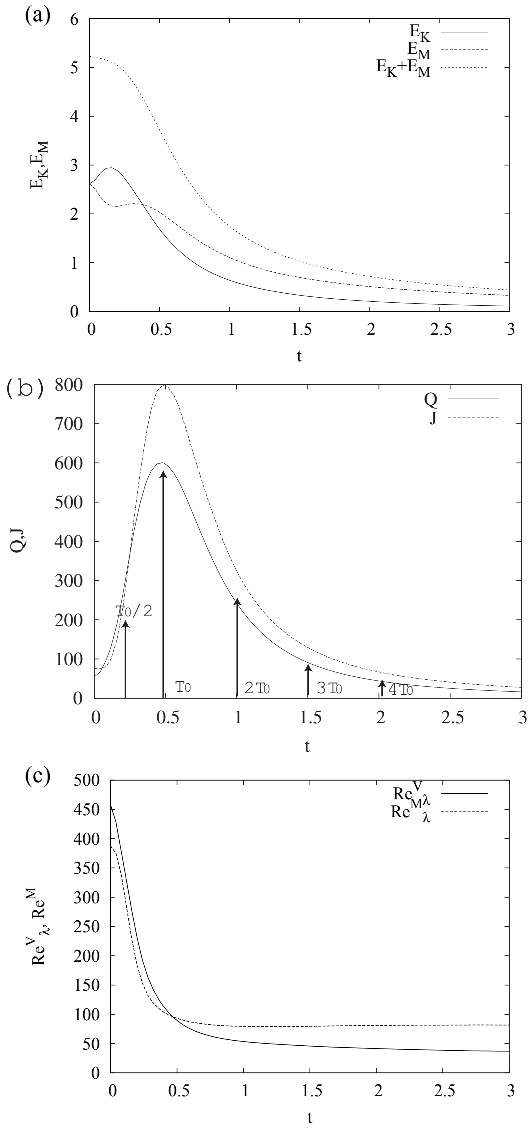

Fig. 1 Time evolutions of (a)E_K, E_M, $E_K=E_K+E_M$, (b)Q and J, and (c)R_λ^V, R_λ^M

$E_K(k)$ and the magnetic energy spectrum $E_M(k)$ are shown at $t=T_0/2$, T_0, $2T_0$, $3T_0$ and $4T_0$, respectively. The former appears to be scaled by $k^{-5/3}$ (the solid line), while the latter appears to be scaled by $k^{-7/3}$ rather than by $k^{-5/3}$. (Refer to Ref. [2, 3] on the examination of the scaling indices by the compensated energy spectra.) The scaling properties of the two spectra look almost unchanged after $t=T_0$. In Fig.2(c), the transfer functions of the kinetic energy and the magnetic energy, T_K and T_M respectively, are plotted at $t=T_0$. The two transfer functions are defined as

$$T_K(k) = \sum_{[\boldsymbol{k}]}\widetilde{V}_i(k)^*\widetilde{A}_i(k), \quad (5)$$

$$\widetilde{A}_i(k) = F\left[-\frac{\partial}{\partial x_j}\left(V_iV_j-B_iB_j\right)\right.$$

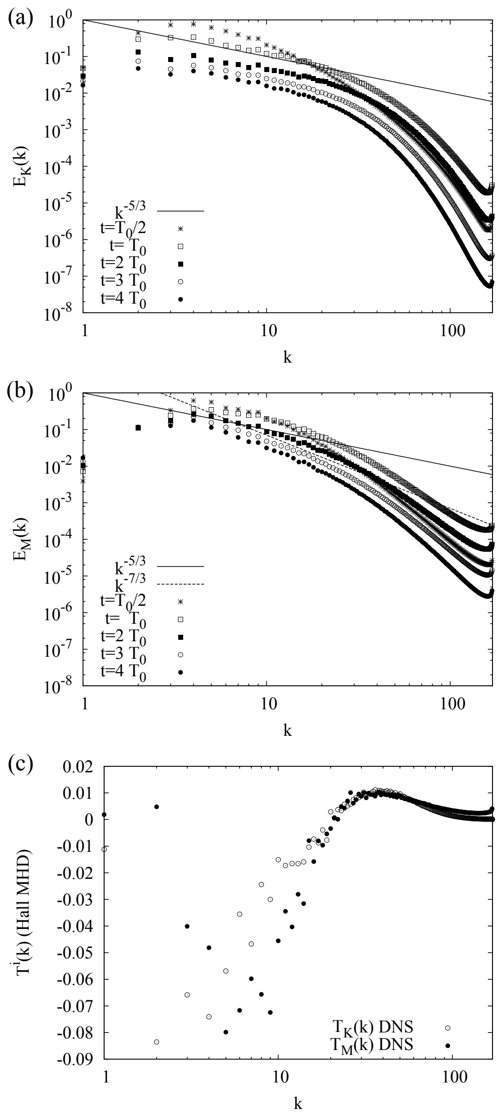

Fig. 2 Time evolutions of (a)the kinetic energy spectrum $E_K(k)$ and (b)the magnetic energy spectrum $E_M(k)$. (c)The energy transfer functions for the kinetic energy $T_K(k)$ and for the magnetic energy $T_M(k)$ at $t = T_0$.

$$-\frac{\partial}{\partial x_i}\left(p+\frac{1}{2}B_jB_j\right)\Bigg], \qquad (6)$$

and

$$T_M(k) = \sum_{[\boldsymbol{k}]} \widetilde{B}_i(k)^* \widetilde{C}_i(k), \qquad (7)$$

$$\widetilde{C}_i(k) = F\Bigg[\epsilon_{ijk} \frac{\partial}{\partial x_j}\left\{\epsilon_{kmn}\left(V_m - \epsilon j_m\right)B_n\right\}\Bigg], \qquad (8)$$

where the symbols $\sum_{[\boldsymbol{k}]}$, $F[]$ and * denote the shell average over the wave number vector $\boldsymbol{k}$, the Fourier transform, and the complex conjugate, respectively. The variables with $\tilde{\cdot}$ are the Fourier coefficients. Here we note characteristics of the two transfer functions $T_K(k)$ and $T_M(k)$ briefly. The kinetic energy transfer function $T_K(k)$ is negative at $k < 20$ and positive at $k > 20$. The profile of $T_K(k)$, negative at low wave numbers and positive in large wave numbers, is quite typical when the forward energy transfer is dominant. On the other hand, the magnetic energy transfer function $T_M(k)$ changes its sign twice. It is positive at the two regions, $k < 3$ and $k > 20$, and negative at $3 \le k \le 20$. There should be the inverse energy transfer toward the first region $k < 3$. The region $3 \le k \le 20$ is considered to be the source of the energy to the other two regions $k < 3$ and $k > 20$.

In Fig.3(a), isosurfaces of the enstrophy density $\Omega^2 = \omega_i\omega_i/2$ are shown. The threshold of the isosurfaces is four times of the deviation above the mean value of Ω^2. In Fig.3(b), isosurfaces of the current density $I^2 = \jmath_i\jmath_i/2$ are drawn by the threshold of four times of the deviation above the mean value. The isosurfaces of both Ω^2 and I^2 exhibit sheet-like structures, as they do in the non-Hall MHD turbulence. However, large-scale structures of the two quantities (especially the enstrophy density) are rather tubular in the Hall MHD turbulence. In fact, the isosurfaces of the two quantities which are drawn only with their Fourier coefficients $k \le 32$, in Fig.3(c), are either elongated ellipsoids or tubes. (The magnetic field lines are also drawn there.) From these observations, we consider that some basic properties of the Hall MHD turbulence are different between large and small scales. For a convenience, we assume $k = 32$ as a wave number to distinguish the large and small scales in this article. Although we do not have a theory to determine the threshold wave number as $k = 32$ uniquely, it is one of a typical scale by which we can find clear change of spatial structures in the processes of visualizations. Hereafter we study turbulent statistics by the use of the low-pass/high-pass filters with $k = 32$ cut-off. For a convenience, we refer to the data with the all Fourier coefficients as the *full resolution* and the data only with $k \le 32$ Fourier coefficients as the *limited resolution*.

3. Statistics w/wo high wave number coefficients

In this section, we study of some statistics with high wave number Fourier coefficients (the full resolution statistics) and without them (the limited resolution statistics). In Fig.4, the probability density function (PDF) of the I^2 at $t = T_0$ is shown both for the full resolution (solid line) and the limited resolution(dashed line), in with the abscissa (a)I^2 and (b)I. While the PDFs of both the full resolution and the limited resolution are concave up in Fig.4(a), they have straight tails in Fig.4(b). It indicates

$$P(I^2) \quad \propto \quad \exp(-I) \qquad (9)$$

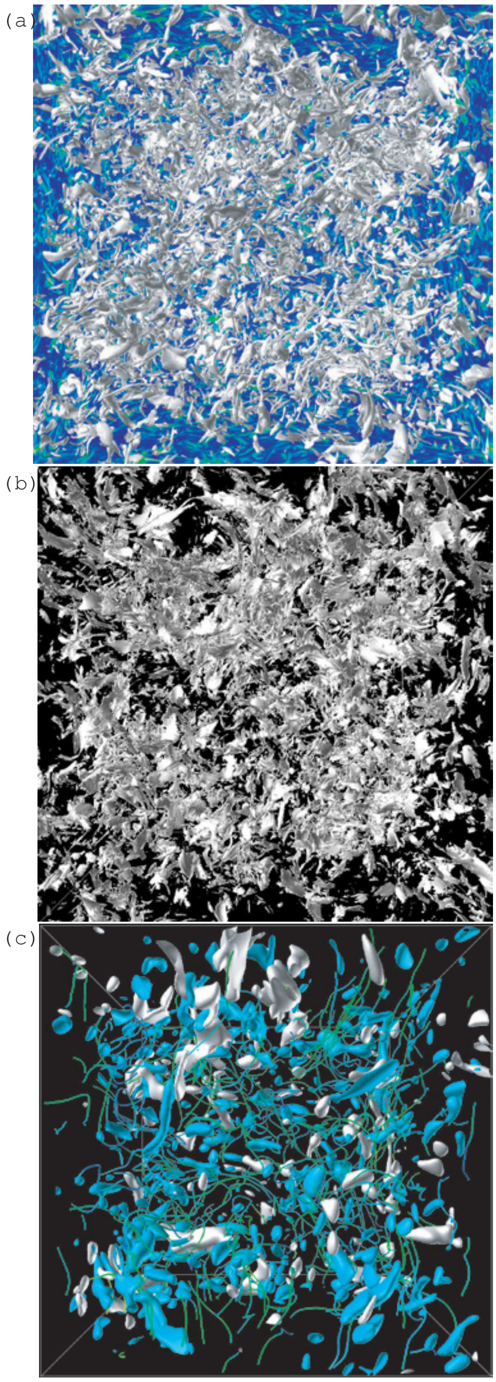

Fig. 3 Visualization of turbulent field. The isosurfaces of (a)the enstorphy density, and (b)the current density for the entire computational box. (c)The isosurfaces of the enstorphy density and the current density, and the magnetic field lines of only $k \leq 32$ Fourier coefficients are drawn.

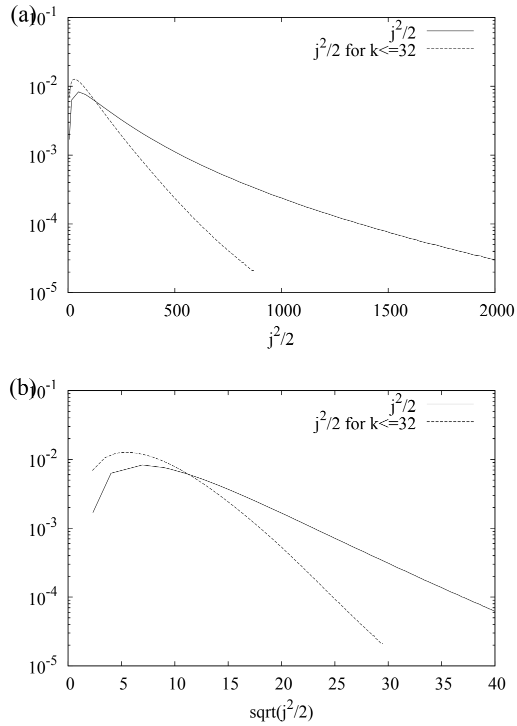

Fig. 4 The PDF of the current density $I^2 = j_i j_i/2$. The abscissa is I^2 in (a) and I in (b).

at large I^2, whether the resolution is full or limited. In Fig.5, the PDFs of Ω^2 of the full resolution and the limited resolution are shown with the abscissa of (a)Ω^2 and (b)Ω. In contrast to the PDFs of I^2, we find that the PDF of the full resolution is

$$P(\Omega^2) \quad \propto \quad \exp(-\Omega) \tag{10}$$

while the PDF of the limited resolution appears

$$P(\Omega^2) \quad \propto \quad \exp\left(-\Omega^2\right). \tag{11}$$

It can be interesting because the PDF of the large scale vortices looks that of a simple Gaussian random field even though they apparently have intermittent vortex structures in Fig.3(c). It is also interesting to find differences between I^2 and Ω^2, because the difference may come from the quadratic nature of the Hall term to the magnetic field, which we miss in the non-Hall MHD equations. In the non-Hall MHD equations, the current density field $\boldsymbol{j}$ and the vorticity field $\boldsymbol{w}$ are closely related with each other through the Elsässer variables $\boldsymbol{V} \pm \boldsymbol{B}$, while they are not in the Hall MHD equations due to the quadratic nature.

Next, we study the alignment of the local vortex structures and the magnetic field lines which is reported first in Ref. [3]. As in the reference, there is a tendency that the magnetic field lines are tangential to the isosurfaces of the enstrophy density. The tendency is investigated here more quantitatively by means of the PDF of the angles between the surface orientation and the magnetic field lines. We can characterize the orientation normal to the surfaces of Ω^2 as the gradient of quantity. The PDF of the angle between the magnetic field lines and the gradient vector,

$$\theta_{B,\nabla\Omega^2} \quad = \quad \cos^{-1}\left(\frac{\boldsymbol{B}\cdot(\nabla\Omega^2)}{|\boldsymbol{B}|\,|(\nabla\Omega^2)|}\right) \tag{12}$$

is shown In Fig.6 for (a)the full resolution and (b)

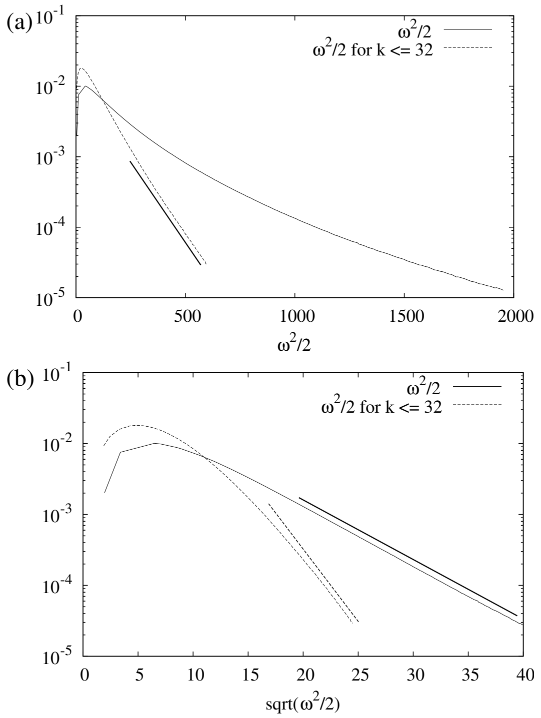

Fig. 5 The PDF of the enstrophy density $\Omega^2 = \omega_i\omega_i/2$. The abscissa is Ω^2 in (a) and Ω in (b).

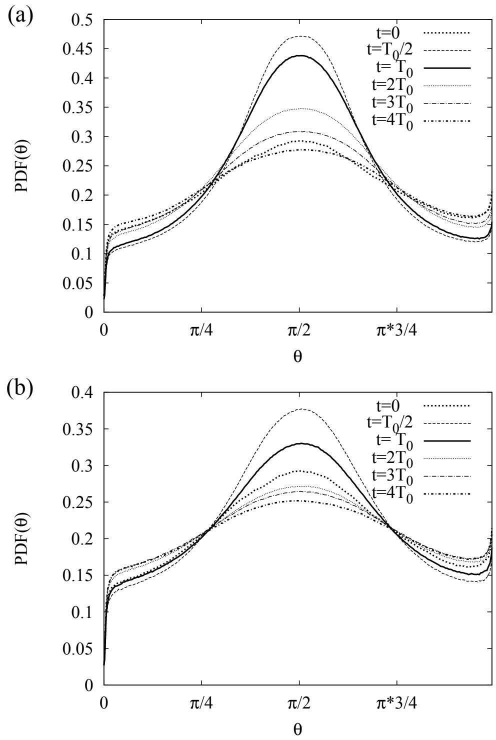

Fig. 6 The angles between the gradient of the enstrophy density and the magnetic field lines of (a) the full resolution and (b) the limited resolution.

for the limited resolution. In Fig.6(a), the PDF at $\theta \simeq \pi/2$ becomes the largest at $t = T_0/2$, in the mid time of the turbulence evolution, and it becomes small rapidly after that. That is, the alignment of the magnetic field lines and the vortex structures are achieved when the turbulence is developing. In Fig.6(b), the PDF for the limited resolution are shown. Though the basic profile of the PDF is similar between the full resolution and the limited resolution, the peaks of the PDFs at the angle $\pi/2$ become less sharp without $k > 32$ coefficients. Our current understanding is that the alignment is contributed mainly by the small scale structures, which are excited in the course of development of the turbulence, and that the alignment is lost when the small scales are dissipated away quickly in the relaxation process.

When we turn our eyes to the relaxation process of $t \geq T_0$, it is natural to consider about the helicity, since it has been considered that the conservation of the helicity can play a key role in the relaxation process in studies of non-Hall MHD turbulence. In the Hall MHD equations, we have three quantities to be conserved in the ideal limit, the total energy

$$E_T = \frac{1}{2}\langle V_i V_i \rangle + \frac{1}{2}\langle B_i B_i \rangle, \tag{13}$$

the magnetic helicity

$$H_m = \frac{1}{2}\langle A_i B_i \rangle \tag{14}$$

where A_i is the vector potential to give the magnetic field by $B_i = \epsilon_{ijk}\partial A_k/\partial x_j$, and the hybrid helicity

$$K = \frac{1}{2}\langle (B_i + \epsilon\omega_i)(A_i + \epsilon V_i) \rangle. \tag{15}$$

In Fig.7, the time evolutions of the three quantities E_T, H_m and K are shown. The total energy E_T, being multiplied by $1/5$ in the figure so that the it can be easily compared to the other quantities, decays quite rapidly while the other two quantities vary relatively slowly. It is reasonable to attribute the difference of the decay rates to their orders of the derivatives, in accordance with a typical selective decay in non-Hall MHD turbulence. Though all the three quantities are not conserved for finite dissipations, their behaviors might give us some insights to understand the statistics in Figs.4, 5 and 6. The conservation of H_m in the ideal limit constrains the behaviors of the magnetic field. The slower decay of H_m than E_T implicitly means that the current density field $\boldsymbol{j}$ is less sensitive than the vorticity field $\boldsymbol{\omega}$ to the dissipations thanks to the constraint. It is consistent with the behaviors of R^V_λ and $R^M_{\lambda'}$ in Fig.1(c), in which the former decays after $t \geq T_0$ while the latter stays almost constant, showing that the small scales in the velocity field are dissipated while those of the magnetic field are kept. It might be a consequence of the insensitive nature that the current density field shows more intermittent structures as in Fig.4(b) than the vorticity field in Fig.5(b), although this remains as a tentative conjec-

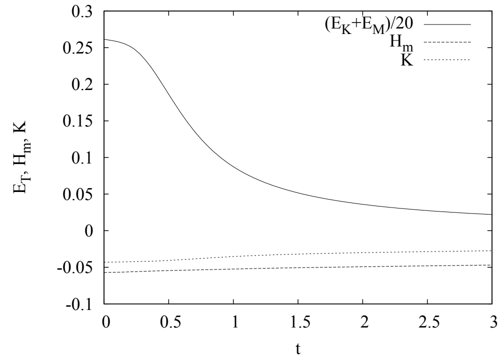

Fig. 7 The time variation of the three quantities $(E_K + E_M)/20$, H_m and K.

ture to be studied. The roles of the helicity and the hybrid helicity in formation/relaxation of local structures should be studied further in next works.

4. Summary

Statistics in Hall MHD turbulence are investigated by making use of the low-pass filter with $k = 32$ cut-off wave number. It is found that vortex structures in the large scales are well characterized by the Gaussian distribution in spite of their intermittent structures. It may help us to construct an eddy viscosity model by making use of some theories for random field. On the other hand, the current density field represents more intermittent statistics than the vorticity field, so that we need further analyses about it. We have also found that the local vortex structures, especially of the small scales, are aligned to the magnetic field lines when the turbulence level is under developing. The alignment is lost in the decaying (relaxation) process, showing dominance of the turbulent field by the helicity and the hybrid helicity. In order to construct numerical models for the magnetic field, we need to take the influences of the helicity conservation effectively.

This research was partially supported by "Application of Fusion Theory to Space Plasmas" under the project of Formation of International Network for Scientific Collaborations at National Institute for Fusion Science (NIFS)/National Institute for Natural Sciences, Japan. The numerical work was performed on the NEC SX-8 "Plasma Simulator", supported by the NIFS collaborative work NIFS09KNXN154.

References

[1] D. Biskamp, *Magnetohydrodynamic Turbulence* (Cambridge University Press, Cambridge, 2003).
[2] D. Hori and H. Miura, Plasma Fusion Res. **3** S1053 (2008).
[3] H. Miura and D. Hori, J. Plasma Fusion Res. SERIES **8** 73 (2009)
[4] S. Ohsaki and S. Mahajan, Phys. Plasmas **11**, 898 (2004).
[5] P. Goldreich and H. Sridhar, ApJ **438**, 763 (1995).
[6] P. Goldreich and H. Sridhar, ApJ **485**, 680 (1997).
[7] J. Cho, A. Lazarian and E.T. Vishniac, ApJ **564**, 291 (2002).